HHS Public Access

Author manuscript

*Nat Immunol*. Author manuscript; available in PMC 2012 September 01.

Published in final edited form as:

*Nat Immunol*. ; 13(3): 272–282. doi:10.1038/ni.2240.

# Body barrier surveillance by epidermal gammadelta TCR

**Grzegorz Chodaczek**, **Veena Papanna**, **M. Anna Zal**, and **Tomasz Zal**[#]

Department of Immunology, The University of Texas MD Anderson Cancer Center, Houston, TX 77030

## Abstract

The surveillance of body barriers relies on resident T cells whose repertoires are biased toward particular γδ T cell receptor lineages according to location. These γδ TCRs were shown to recognize stress-emergent ligands. Using intravital dynamics-immunosignal correlative microscopy, we report that epidermal T cell-expressed Vγ5 TCRs were constitutively clustered and functionally activated *in vivo* at steady-state, forming bona-fide immunological synapses that polarized and anchored T cell projections at squamous keratinocyte tight junctions. This synaptogenesis depended on TCR variable domains, Lck and αE(CD103)β7-integrin, but not the γδ lineage or NKG2D. In response to tissue stress, TCR-proximal signals did not increase significantly but underwent stress mode-dependent re-localization. Thus, the γδ TCR orchestrates barrier surveillance pro-actively, presumably by recognizing steady-state-expressed tissue ligands.

Environment-exposed epithelia, such as those lining the gastrointestinal, reproductive and bronchoalveolar tracts, as well as the skin, are under the surveillance of resident T cells predominantly expressing γδ TCRs. Without these γδ T intraepithelial lymphocytes (γδ IELs), body barriers are easily compromised: *Tcrd*$^{-/-}$ (γδ TCR-deficient) mice are susceptible to carcinogenesis[1], impaired wound healing[2], experimental colitis[3] and strain-dependent permeability deregulation[4]—all despite the presence of IELs expressing αβ TCRs. Although the importance of γδ IELs and their TCRs in body barrier homeostasis is well established, the exact roles of γδ TCRs *in vivo* remain controversial and their physiological ligands are unknown.

Unlike in the highly polyclonal αβ T cells, whose TCRs recognize diverse peptide-loaded cell surface MHC molecules, intraepithelial γδ TCRs are MHC-independent and distinctly oligoclonal in a manner that depends on the organ. For example, the $V_\gamma1J_\gamma1C_\gamma1$-$V_\delta1$ heterodimers in humans, and the orthologous $V_\gamma7$-$V_\delta1$ heterodimers in mice (Tonegawa's nomenclature) are over-represented in the intestine, and in mice the $V_\gamma6$-$V_\delta1$ heterodimers dominate the reproductive tract mucosa and the $V_\gamma5$-$V_\delta1$ heterodimers are characteristic for the epidermis[5, 6]. Because of this location-dependent $V_\gamma$ chain bias, which is only in part



[#]Correspondence: tzal@mdanderson.org.

**Author contributions**

GC and TZ designed the studies, analyzed and interpreted the results, and wrote the manuscript; GC acquired most data; VP and MAZ assisted and acquired some data.

The authors declare no conflict of interest.

attributable to the sequential rearrangements of $V_\gamma$ gene segments in neonatal thymocytes, and considering that this bias is unaffected in germ-free mice, it has been hypothesized that epithelial γδ TCRs recognize the healthy host tissue[7].

However, extensive evidence indicates that epithelial γδ TCRs are used for recognizing cells that are affected by stress, such as that due to trauma or malignancy[8, 9]. Stress recognition can also be mediated through the NK cell family receptor NKG2D, which binds the stress-upregulated proteins of the Rae family[1, 10, 11]. Thus, epithelial γδ TCRs are thought to serve as stress ligand receptors, perhaps by complementing NKG2D[1, 12, 13].

The characteristically shaped murine dendritic epidermal T cells (DETCs), which are derived from the first wave of $V_\gamma$ locus rearrangements and selected in the embryonic thymus depending on the butyrophilin-family protein Skint1[14-16], express almost exclusively the $V_\gamma5$-$V_\delta1$ TCR, which was shown to be important for the recognition of stressed and cancerous cells *in vitro* and tissue homeostasis *in vivo*[1, 2, 9, 17]. As such, DETCs represent a stringent model for investigating the significance of γδ TCR invariance in epithelia. Given that *Tcrd*$^{-/-}$ mice do contain DETCs that express diverse αβ TCRs, γδ TCR is not critical for the colonization of epidermis by DETCs; however, the αβ DETCs in *Tcrd*$^{-/-}$ mice do not persist[17]. This phenomenon could be attributable to an intermittent stimulation of the canonical DETC TCR by stress ligands[17], but is also consistent with the healthy tissue recognition hypothesis[18-20].

To investigate the biological significance of epithelial γδ TCR invariance, we studied the *in vivo* interactions of DETCs using a novel imaging approach that allowed us to relate single-cell dynamics to the subcellular compartmentalization and signaling by TCR and other molecules within the same cells *in situ*. Here, we show *in vivo* that the epidermal TCR is not idle at steady state, but is continuously engaged in an activatory, body barrier-targeted synaptic interaction. Our findings suggest a surveillance mechanism whereby γδ TCRs recognize physiologically expressed self-ligands.

## RESULTS

### DETCs are anchored in the apical epidermis through PALPs

To relate the dynamics of DETCs to the states of TCR compartmentalization and signaling *in situ*, we recorded DETC dynamics by 3D resonant scanning confocal microscopy in the ear of IL-2p8-GFP transgenic reporter mice, in which an 8.4-kb regulatory fragment of the murine interleukin 2 (IL-2) gene drives high-level expression of the green fluorescent protein (GFP) in DETCs[21]. Immediately following the recording, full-thickness skin was harvested and fixed avoiding mechanical and chemical separation of epidermis and then stained with various combinations of fluorescence-labeled antibodies. The resulting immunofluorescence confocal data was co-registered with the *in vivo* motility recordings by *in silico* landmark identification and affine alignment, allowing for the *in vivo* cell dynamics to be related to a variety of molecular signals in the same cells.

Using this technique, termed intravital dynamics-immunosignal correlative (iDISC) microscopy, to inspect DETCs in healthy reporter mice bred on the C57BL/6 wild-type

background, we found that as many as 71% of these cell's dendrites were oriented at right angles toward the apical epidermis where they were immobilized at distal, cytoplasm-filled bulbous swellings (Fig. 1a, b and Supplementary Fig. 1,Supplementary Video 1). In any given 1 h time period, a typical wild-type DETC had three, and some as many as seven, dendrites that were apically-anchored (Fig. 1b). The remaining dendrites were positioned within the basal epidermis and were highly mobile, extending and contracting with leading edge velocities of, respectively, 0.59±0.05 (n=33) and 0.78±0.06 μm/min (n=30). Rapid fixation of intravitally monitored skin (as well as unmanipulated control skin) showed that the ends of the apically oriented dendrites contained prominent co-clusters of TCR and proteins phosphorylated on tyrosines (pY) (Fig. 1a, c and Supplementary Video 2 and 3). Quantitatively, the pY signals, whose specificity was verified by phosphatase pre-treatment (Supplementary Fig. 2), were several times as strong at the ends of the apical/immobilized dendrites as at the ends of the basal/motile ones (Fig. 1d). We termed these pY-containing structures phosphotyrosine-rich aggregates located on projections (PALPs). When the immunofluorescence confocal volumes were aligned with the intravital video recordings, the PALPs invariably co-localized with the apical dendrite anchoring sites (Fig. 1a; Supplementary Video 3). These results indicate that DETCs interact with the host tissue in a highly characteristic manner that was associated with TCR and pY signal polarization.

## $V_\gamma5$ TCR and rare αβ TCRs mediate PALP formation

Given the spatiotemporal correlation between the anchoring of dendrites and the clustering of TCR in the PALPs, we asked whether this interaction was reflective of ligand engagement by the epidermal $V_\gamma5$ TCR. To this end, we investigated the behavior, TCR distribution and pY content in DETCs lacking γδ TCRs, but expressing polyclonal αβ TCRs, which populate the epidermis in *Tcrd*$^{-/-}$ mice. In IL2p8-GFP reporter mice that were back-crossed onto syngeneic *Tcrd*$^{-/-}$ background, most dendrites in αβ DETCs were motile and were not preferentially directed at the apical epidermis (Fig. 1a, b; Supplementary Video 3 and 4). Furthermore, anti-CD3ε antibody bound uniformly along these cell's membranes, revealing almost no TCR polarization towards dendrite endings (Fig. 1a, c, e), and only weak pY signals were detectable in foci dispersed along cell bodies, but not in PALPs (Fig. 1a, c, f). In addition, we looked for naturally occurring $V_\gamma5^-$ CD3ε$^+$ DETCs in wild-type skin using epidermal localization, dendritic morphology and differential binding of anti-$V_\gamma5$ and anti-CD3ε antibodies as identification criteria (Fig. 1g). As shown later, at least some of these cells expressed non-$V_\gamma5$ γδ TCRs. In contrast to $V_\gamma5^+$ DETCs, non-$V_\gamma5$ DETCs largely lacked dendrite-terminal TCR polarization and PALPs (Fig. 1eg), their dendrites were not anchored, and some of these cells were migratory (Fig. 1h, i; Supplementary Video 5, and data not shown). Taken together, these findings indicated that the anchoring of dendrites and formation of PALPs depended on the composition of TCR heterodimer in a manner that correlated with the $V_\gamma5$ TCR.

However, an extensive survey of *Tcrd*$^{-/-}$ skin revealed rare, clone-like groups of αβ DETCs that resembled the wild-type DETCs with respect to the pattern of TCR and pY polarization as well as dendrite immobilization (Supplementary Fig. 3). To verify that the wild-type-like morphology of rare αβ DETCs depended on the specificity of their αβ TCRs, we limited the TCR repertoire to only one, ovalbumin 257-264/H2-K$^b$-specific αβ TCR by using the OT1

TCR transgenic mice bred on the Rag-1-deficient background (OT1 *Rag1*$^{-/-}$)[2, 22, 23]. In DETCs that were present in these mice, TCR was not polarized, PALPs were deficient, and, importantly, no wild-type-like DETCs could be found (data not shown). Thus, while the steady-state formation of PALPs is an attribute of the $V_\gamma5$ TCR, it can be mimicked to some extent by rare αβ TCRs. Consequently, the dependence of this interaction on the TCR variable domain, rather than its lineage, suggests that the formation of PALPs is driven by TCR binding by a ligand.

## The steady-state apical PALPs are long lived

To determine the stability of the PALPs, we assessed the same DETCs twice a day in wild-type reporter mice over a period of 28 days. Overall, most DETCs remained anchored, and some disappeared—their fate uncertain—while other divided, which is consistent with homeostatic self-renewal (Supplementary Fig. 4a; Supplementary Video 6). In the dividing cells, dendrites detached and cell bodies rounded up, showing that PALPs could orderly disassemble. Interestingly, the newly divided daughter cells migrated slowly in a directional manner for several days prior to settling in nearby unoccupied sites and forming new, apically attached dendrites (Supplementary Fig. 4a-c **and** Supplementary Video 6). The kinetics of dendrite detachment conformed to the single exponential decay model with a half-life of 60 h, and some anchorages persisted for as long as 17 days (Fig. 1j and Supplementary Fig. 4d, e). By comparison, while in wild-type mice on average 2.1 dendrites per DETC were found at the same positions after 24 h, in *Tcrd*$^{-/-}$ mice, only 0.4 dendrites per cell were found so, which were not followed further (Fig 1j). Thus, the PALPs were remarkably stable, yet homeostatically regulated.

## $V_\gamma5$ TCR targets DETCs at the squamous keratinocyte junctions

To determine the localization of PALPs within the epidermis, we stained it for the markers of keratinocyte stratification, namely F-actin, which is enriched along the most apical squamous keratinocyte junctions in stratum granulosum layer 1 (SG1), and zona occludens-1, a constituent of the SG2 tight junctions. We found that PALPs were located almost exclusively along the squamous keratinocyte junctions, often at the triple junctions (Fig. 2a, b). In the vertical dimension, they were located below the SG1 junctions and at or just below the SG2 junctions (Fig. 2c). Because tricellulin, a characteristic component of the triple tight junctions[24], was absent along dendrites and in the PALPs (but as expected was present in the triple inter-keratinocyte junctions), it was unlikely that the apical dendrites protruded into the stratum corneum (Fig. 2d and data not shown). Furthermore, this analysis revealed that PALPs coincided with distinct foci of F-actin, which were readily detectable above the already high concentration of F-actin along squamous keratinocytes in wild-type, but were absent in *Tcrd*$^{-/-}$ mice. Consistently, only a few apical dendrites terminated at the squamous keratinocyte junctions in *Tcrd*$^{-/-}$ mice (Fig. 2e, f). Thus, DETCs were targeted through the PALPs at the barrier-forming tight junctions and were enriched in F-actin, whose clustering along squamous keratinocyte junctions could, therefore, be used as an alternative PALP's marker.

## PALP formation does not require signals from NKG2D

Besides through the $V_\gamma5$ TCR, DETC can be activated through NKG2D, a well documented stress ligand receptor[1, 10, 11]. We evaluated the role of NKG2D in PALPs using mice lacking both the DAP10 and DAP12 chains that are used by NKG2D for signaling in mice[25]. Using the steady-state TCR and actin clustering as surrogate PALPs indicators (pY could not be assessed owing to different fixation protocol and specimen transportation), we found that both of these features were unaffected in the DAP10-DAP12-deficient mice (Fig. 2e, f). In addition, NKG2D was not enriched at the ends of dendrites, but localizing intracellularly (Fig. 2g and Supplementary Fig. 5a, b). Therefore, the steady-state apical tight junction targeting did not require NKG2D (or any other DAP10 and/or DAP12-dependent receptors).

## PALPs are the sites of Lck-mediated $V_\gamma5$ TCR activation

Considering that TCR was aggregated coincident with protein tyrosine phosphorylation, which often mediates receptor signaling, including by TCR, we investigated whether TCR in PALPs was activated. The recognition of a cognate antigen by TCR triggers a characteristic signaling cascade that begins with the phosphorylation of the immune tyrosine activatory motifs in the TCR-associated CD3 chains by the Src-family kinases (SFKs), predominantly by Lck, and is followed by the recruitment and phosphorylation of the ZAP70 protein that transduces TCR signals intracellularly[26, 27]. Using sequence-specific anti-phosphotyrosine antibodies, we found that the termini of apical dendrites contained high levels of CD3ζ chains phosphorylated on Tyr142 ($pY^{142}$-CD3ζ), which is indicative of TCR binding by agonist ligands[27] (Fig. 3a). As control, only background signals could be discerned in CD3ζ-deficient DETCs (which are sustained by the homologous FcεR1γ chains) (Supplementary Fig. 6a). The dendrite-terminal TCR-CD3ζ phosphorylation was evident in various mouse strains, consistent with MHC-independency (Supplementary Fig. 6b, c), and was unaffected in germ-free mice (Supplementary Fig. 6d). Moreover, the apical terminations were enriched in the catalytically active, Tyr418-phosphorylated forms of the SFKs and Tyr493-phosphorylated ZAP70, indicative of signal propagation (Fig. 3a, b). Upon treating freshly harvested skin fragments with PP2, a broad SFK inhibitor, or '428205', an inhibitor specific for Lck (or the inactive PP3 control), both PP2 and 428205 (but not PP3) decreased the $pY^{142}$-CD3ζ levels in DETCs several fold within 3 h (Fig. 3c). In addition, Lck inhibition with 428205 provoked DETC rounding (Fig. 3d). Thus, the $V_\gamma5$ TCR in PALPs was activated in a manner dependent on Lck and independent of environmental microbiota.

To determine the dependence of steady-state *in vivo* TCR signaling in DETCs on TCR, we examined the $pY^{142}$-CD3ζ and $pY^{418}$-SFK signals in *Tcrd*$^{-/-}$ mice. Unlike in wild-type mice, only low steady state $pY^{142}$-CD3ζ and $pY^{418}$-SFK signals could be detected at the ends of most αβ DETC dendrites, and the whole cell $pY^{142}$-CD3ζ levels were also lower (Fig. 3e, f). The αβ TCRs in *Tcrd*$^{-/-}$ DETCs were functional and available for binding, as indicated by the extensive CD3ζ-$Y^{142}$ phosphorylation upon *in vivo* cross-linking of TCR-CD3 complexes with intradermally-injected biotinylated anti-CD3ε antibody and streptavidin (Supplementary Fig. 7a). Nevertheless, the diminished TCR activity in *Tcrd*$^{-/-}$ DETCs could represent an indirect effect, such as disturbed homeostasis, as opposed to the lack of $V_\gamma5$-like antigen specificity by αβ TCRs. To investigate this scenario, we supplemented newborn *Tcrd*$^{-/-}$ mice with day 14-16 fetal thymocytes from wild-type

IL2p8-GFP donors to generate chimeras containing less than 0.1% $V_\gamma5^+$ $GFP^+$ DETCs in an αβ DETC-inhabited epidermis. The donor-derived, $V_\gamma5^+$ DETCs, but not the neighboring, host-derived (αβ) DETCs contained high levels of $pY^{142}$-CD3ζ chains in apically-positioned dendrite terminations (Supplementary Fig. 7b), underscoring the importance of $V_\gamma5$ TCR in PALPs and excluding microenvironmental effects or ligand unavailability as the causes of PALP's deficiency in *Tcrd*$^{-/-}$ mice. Consistent with these results and with the notion that certain αβ TCRs could recognize apically localized activatory ligands, the apical TCR clusters that were observed in rare wild-type-like αβ DETCs in *Tcrd*$^{-/-}$ mice were CD3ζ-$Y^{142}$-phosphorylated (Supplementary Fig. 3b-e).

Next, we compared the *in situ* TCR signals between the rare naturally occurring non-$V_\gamma5$ γδ $TCR^+$ DETCs and their $V_\gamma5^+$ neighbors. Almost no $pY^{142}$-CD3ζ was detectable at the ends of dendrites in non-$V_\gamma5$ γδ DETCs (Fig. 3g), although they contained comparable $pY^{142}$-CD3ζ levels as the $V_\gamma5^+$ DETCs when these signals were integrated over the whole cells, consistent with signal delocalization, perhaps reflective of the recognition of alternative ligands (Fig. 3h). Taken together, the presence of agonistic TCR-proximal signals in $V_\gamma5$ DETCs at steady state, and the dependence of these signals' strength and subcellular patterning of on TCR heterodimer composition suggest that the epidermal $V_\gamma5$ TCR is a physiologically autoreactive TCR.

## Steady-state TCR signals result in DETC pre-activation

We next investigated whether the *in vivo* steady-state TCR-proximal signals were effective in DETC activation. DETCs freshly isolated from healthy wild-type mice expressed the cell surface activation marker CD69 at levels that were higher than on *Tcrd*$^{-/-}$ αβ DETCs (Fig. 3i). CD69 levels on wild-type DETCs decreased when the cells were cultured in dispersion, which also abolished CD3ζ tyrosine phosphorylation and, as expected, were maintained in the presence of TCR cross-linking (Fig. 3i and data not shown). Furthermore, taking advantage of the IL2p8-GFP reporter transgene, which is inducible in peripheral T cells upon activation[21], we investigated if its high *in vivo* activity in wild-type DETCs was actively maintained by TCR, for which we compared the levels of GFP in DETCs in wild-type or *Tcrd*$^{-/-}$ reporter mice. Consistent with CD69 expression, GFP levels in DETCs were higher in wild-type than in *Tcrd*$^{-/-}$ IL2p8-GFP reporter mice, as determined by flow and image cytometry (Fig. 3j, k), and whereas the GFP fluorescence in wild-type DETCs remained high when in culture in the presence of TCR cross-linking, it decreased upon DETC dispersal (Fig. 3k). As expected, the low levels of GFP in IL2p8-GFP *Tcrd*$^{-/-}$ DETCs increased upon TCR cross-linking (Fig. 3k). Together, these results indicated that the *in vivo* $V_\gamma5$ TCR signals were functional in maintaining DETCs in a state of steady activation.

## Dendrite anchoring through PALPs is modulated by CD103 integrin

To explore the mechanism of dendrite immobilization, we investigated the role of the epithelial integrin $\alpha_E$(CD103)$\beta_7$, which is expressed by DETCs and regulates their morphology[28, 29]. Despite the presence of its ligand, E-cadherin, across the epidermis (data not shown), CD103 was highly enriched at the ends of apical dendrites, colocalizing with the PALPs (Fig. 4a, b). In contrast, CD103 was more evenly distributed in the αβ DETCs in

*Tcrd*$^{-/-}$ mice (Fig. 4c, d), in which, unexpectedly, the whole-cell levels of CD103 were higher than in wild-type controls (Fig. 4c, e). In CD103-deficient mice, dendrite-terminal γδ TCR clustering and CD3ζ tyrosine phosphorylation were unperturbed (Fig. 4c, f), but significantly fewer dendrites were anchored (Fig. 4g). Besides the CD103 integrin, PALPs were also enriched in the $\alpha_L\beta_2$ integrin LFA-1 (Supplementary Fig. 8a, b), whose levels in wild-type and *Tcrd*$^{-/-}$ DETCs were similar (Supplementary Fig. 8c, d). Although we did not generate reporter mice deficient both in CD103 and LFA-1, these data are consistent with a mechanism by which TCR regulates dendrite attachment through CD103 and possibly additional integrins, such as LFA-1.

## PALPs resemble immunological synapses

To explore if PALPs represent immunological synapses (IS), which are distinctly patterned T cell-target signaling interfaces that provide directionality to T cell effector function[30], we imaged individual PALPs by 3D confocal microscopy at the highest, diffraction-limited resolution. We found that PALPs consisted of multiple tyrosine-phosphorylated microclusters that in wild-type mice on the C57BL/6 background were distributed according to four distinct patterns: the 2 to 4 μm wide “rings” (40 ± 4%), which localized along the perimeter of bulbous swellings; the “elongated” PALPs (23 ± 4%), which typically were oriented perpendicular to dendrite shafts and in alignment with inter-keratinocyte junctions; the “platform” PALPs (21% ± 3%) that were filled evenly with pY microclusters; and finally the small, “focused” PALPs (15% ± 2%) (Fig. 5a). Considering that the representation of PALP forms was strain-dependent, for example, the elongated PALPs predominated in AKR mice (Supplementary Figs. 6b, c and data not shown), the underlying interaction was genetically regulated. In the ring PALPs, TCR was distributed in the periphery in diffuse overlap with the pY microclusters, which was reminiscent of an early stage αβ T cell IS, and, in about 37% of the ring PALPs, additional TCR was present in a central, cytoplasm-immersed pY-free cluster, which resembled the central supramolecular activatory cluster (cSMAC) that in the ‘mature’ IS is the site of TCR internalization[30] (Fig. 5b, c). The signaling intermediates: pY$^{142}$-CD3ζ, pY$^{493}$-ZAP70 and pY$^{418}$-SFKs were all localized in the peripheral ring and not in the central TCR cluster; therefore, the former represents the zone of TCR activation (Fig. 5d, e). Like in the ring PALPs, some elongated PALPs contained a pY-free TCR microcluster (Supplementary Fig. 6c), indicative of topological similarity between these seemingly different forms. In the rare wild-type-like DETCs that were found in *Tcrd*$^{-/-}$ mice, PALPs were organized like their ring-shaped or platform-shaped $V_\gamma5$ prototypes, hinting that the corresponding ligands were similarly positioned (Supplementary Fig. 3c, d).

A characteristic feature of the classical immunological synapse is the partial exclusion of CD45, a cell membrane protein tyrosine phosphatase that regulates TCR signaling in part by segregating from it in the IS[31]. In PALPs, CD45 was largely excluded from the peripheral ring and accumulated inside it (Fig. 5h and Supplementary Fig. 9a, b). The CD45-TCR separation was also evident in the elongated PALPs, the CD45/TCR ratios decreasing towards the ends of the apical but not the non-apical dendrites. Since the CD45/TCR membrane density ratios were uniform in DETCs cultured *in vitro* (Supplementary Fig. 9c), the CD45-TCR segregation is actively maintained by an interaction with the tissue.

Functionally, the classical IS mediates directional trafficking of intracellular cargo[32]. We visualized intracellular granules both in the fixed skin by using the lysosomal marker LAMP-1 or the lipid raft-endosomal-exosomal component ganglioside GM1[33, 34], as well as *in vivo* by using the acidic granule dye LysoTracker Red DND-99, and found that these cargo were heavily polarized toward the PALPs and distinct from the central TCR clusters (Fig. 5i-k). Overall, we concluded that PALPs were both structurally and—considering the immobilization and vesicular cargo polarization—functionally similar to the early-intermediate immunological synapses.

## Trauma and inflammation promote TCR signal redistribution

To investigate the role of γδ TCR in DETC response to tissue stress, we inflicted damage upon the skin by full thickness wounding, which in agreement with prior reports[2, 11] triggered DETC rounding. Whereas in wild-type mice the zone of DETC rounding extended only 180 μm from the wound borders, it reached as far as 500 μm in *Tcrd*$^{-/-}$ mice (Fig. 6a, b), indicating that $V_{\gamma}5$ TCR signals acted to stabilize the apical outreach under stress. In the wound-proximal DETCs in wild-type mice, cell rounding began after 1 h, at which time the apical dendrites and PALPs still remained, consistent with a preferential retraction of the non-apical dendrites (Fig. 7a, b). Importantly, this process was paralleled by the emergence of new pY$^{142}$-CD3ζ signals, first on the apical cell surfaces and, at 24 h, in the basal epidermis in clusters all around the cell bodies, as evident in a 10-fold increase in the mid-body pY$^{142}$- CD3ζ levels compared to the steady state (Fig. 7a-c). The whole-cell pY$^{142}$-CD3ζ levels, however, did not increase significantly in the course of this response and dropped to near one half of the steady-state levels after 72 h (Fig. 7b, d). At that time, new dendrites emerged that exhibited vigorous tissue probing action (Fig.7a, e-h and Supplementary Video 7). To fine-tune the strength of tissue stress, we applied to the skin titrated amounts of the topical irritant phorbol 12-myristate 13-acetate (PMA). Whereas at a high PMA concentration (100 μg/ml), the skin-resident DETCs rounded up within 4-5 h and stayed so after 24 h, at a low PMA concentration (20 μg/ml), DETCs transitioned directly to the probing stage (Fig. 7e, f and Supplementary Video 7). However, DETCs did not round up when only their TCR was stimulated selectively by intravital cross-linking with intradermally injected anti-CD3ε biotinylated antibodies and streptavidin, which as previously mentioned, was effective in causing γδ TCR clustering and CD3ζ phosphorylation (Supplementary Fig. 7a, data not shown). Taken together, these results showed that TCR signals acted consistently to promote cell membrane attachment, and that tissue stress triggered a basolateral TCR signal de-localization, attachment-freeing PALP's disassembly and, upon variable delay, increased tissue probing action.

## Inflammation induces basal PALPs and DETC-Langerhans cell synapses

To mimic a non-trauma inflammatory stress akin to viral infection, we injected the dermis with unmethylated CpG-containing oligonucleotide A (CpG-A), an agonist of Toll-like receptor 9 (TLR9), which as expected caused epidermis swelling within 3 days. Under these conditions, a number of DETCs extended single dendrites towards the dermis-epidermis junction. The ends of these basal dendrites contained high concentrations of TCR that was phosphorylated on Tyr142 inCD3ζ, thereby defining the basal PALPs (Fig. 8a and Supplementary Video 8). The intensity of pY$^{142}$-CD3ζ signals in the basal PALPs was

three-fold higher than in the apical, steady state PALPs, and yet, owing to only one basal PALP forming per cell, the whole-cell $pY^{142}$-CD3ζ levels were not higher than those at steady-state (Fig. 8b). The basal PALPs were also found near inadvertently inflamed wounds, indicative of physiological relevance. The intravital dynamics-immunosignal correlative imaging showed that like the apical PALPs, the basal PALPs mediated dendrite attachment (Fig. 8c). Furthermore, we found that in TLR9-inflamed skin some DETCs formed stable conjugates with Langerhans cells (LC), in which the contact interfaces contained highly polarized $V_\gamma5$ TCR as well as $pY^{142}$-CD3ζ chains (Fig. 8d, e, Supplementary Video 9). As such, the DETC-LC interaction represented yet another DETC TCR synapse-like signaling pattern. So far, we failed at triggering or maintaining DETC activation, as judged by CD69 and reporter GFP expression, or CD3ζ phosphorylation, in *in vitro* DETCs co-cultured with LCs that were freshly isolated from CpG-A-treated skin, or with immature, differentiated or cancerous keratinocytes (with or without IL-2, and in contrast to control anti-TCR antibody cross-linking) (data not shown). This suggested that the putative $V_\gamma5$ TCR ligands that may activate DETCs at steady state or in response to tissue stress *in vivo* are only indirectly associated with such cells and/or labile. Altogether, our analysis of *in vivo* DETC responses to mechanical or inflammatory stress showed that the steady-state TCR activation that mediated DETC apical polarization and tight junction-proximal attachment through the apical PALPs was poised for remarkably varied, stress-mode-dependent spatiotemporal re-organization.

## DISCUSSION

The role of epithelial γδ TCRs in generating activatory signals upon recognizing yet unknown stress antigens that emerge in response to tissue or cell malfunction has been previously demonstrated. Here we show that epidermal γδ TCRs are also engaged in a steady-state activatory interaction through distinct synaptic structures. Given the distinct localization of the PALPs, our results suggest that besides stress-emergent ligands, the epidermal γδ TCR recognizes a physiologically expressed ligand that at steady-state is compartmentalized in the apical epidermis near the squamous keratinocyte tight junctions.

The observed clustering and signaling by $V_\gamma5$ TCR in the PALPs could also be mediated by a non-ligand mechanism, for example by a lateral association with other receptors. In such case however, the spatial pattern of those signals would depend on the γδ or αβ TCR lineage, and not depend on the heterodimer composition within each lineage. The observed differences between the $V_\gamma5^+$ DETCs and the endogenous non-$V_\gamma5$ γδ DETCs in unmanipulated mice, as well as the rare $V_\gamma5$-like DETCs found amongst the polyclonal αβ DETCs in *Tcrd*$^{-/-}$ mice, but not amongst the monoclonal OT1 αβ TCR-transgenic DETCs, strongly suggest a ligand-binding interpretation of this data. Another possible explanation is that TCR signaling in PALPs is triggered by a closely associated co-receptor that is present only in $V_\gamma5^+$ DETCs. We consider this scenario as highly unlikely. Future identification of the physiological TCR ligands will address these issues.

Based on these findings, the search for the steady-state $V_\gamma5$ TCR ligand should focus on the apical, squamous epidermis and include keratinocyte maturation markers. Considering the spatiotemporal realignment of TCR signals upon stress, and the lack of TCR activation in

DETCs contacting purified target cells *in vitro* (data not shown), we think that the putative steady-state ligand is, in a broad sense, labile in response to tissue stress. By this, we mean that it could either physically detach from its peri-tight junction localization, or it could cease to interact with TCR by other mechanisms, for example, through its degradation, internalization or chemical modification. While it is also possible that the apical TCR signals could be quenched by signals from other receptors while the apical ligand itself remains unchanged, the concomitant emergence of alternatively patterned TCR signals is less readily explained by this mechanism. The transition of TCR signals from the apical to basal epidermis could reflect a migration of detached ligand molecules and redisplay on other cells, including Langerhans cells. Alternatively, sub-apical cells could begin expressing new, perhaps distinct ligands. One attractive candidate for the steady state ligand is Skint1, which not only selects DETCs in the thymus but is also present in the epidermis and is protease-sensitive[15, 16]. Evaluating Skint1 and its epidermal associates, as well as other ligand candidates is a subject of ongoing investigation.

We propose that TCR binding by a physiologically-present, apically confined ligand maintains IELs in a state of spatially targeted, yet incomplete activation. One role for this pre-activatory targeting is to enhance the surveillance of the apical, barrier-forming tight junctions while sensitizing T cells to additional stimulation. In this respect, our findings dovetail with the recent report of the costimulatory role of the DETC cell surface receptor JAML, whose ligand, CAR, is sequestered at steady-state on the apical side of tight junctions[35]. It seems that γδ TCR may act as a pre-activatory synapse positioner to facilitate the exposure of JAML to CAR upon tight junction disruption. This surveillance mechanism is consistent with the two signal theory of T cell activation[36], whereby a second, costimulatory signal is necessary for full activation, as well as with a prior model of DETCs pre-activation[11]. According to our model, however, it is TCR that generates these pre-activatory signals and, more importantly, it does so continuously by interacting with a physiologically expressed ligand, rather than with an intermittent, stress-induced one.

In the light of this report, another newly identified role for the epidermal TCR is to monitor the spatial pattern of the putative ligand. Indeed, we have defined altogether four distinct $V_\gamma5$ TCR signal distribution patterns: the steady-state apical PALPs; the mid-body microclusters that transiently emerge upon sterile trauma; the basal PALPs and the DETC-LC synapses. We did not detect large increases in the whole cell $pY^{142}$-CD3ζ levels, but rather a signal decrease, suggesting that the subcellular patterning and outside context of TCR signals rather than the whole-cell level of TCR signals is of primary importance. Nevertheless, a possibility remains that we failed to detect transient TCR proximal signals that lasted less than the 1 h temporal resolution of this study. Alternatively, stress-activated TCR could generate qualitatively different signals. Likewise, it cannot be excluded that even very small increases in whole-cell levels of TCR signals are biologically significant.

In support of our notion that the steady-state TCR signals are functional, we have shown that the apical PALPs bear a striking resemblance to the early-intermediate αβ T cell synapses[37]. Given that the apical PALPs are filled with lysosomal and other cargo, we speculate that they may participate in intercellular communication, including a rapid and spatially pre-oriented secretory function. For example, DETCs could use PALPs to regulate epithelial cell

turnover by secreting cytokines[4, 38], such as the IGF-1[39], or directly kill cancerous cells using granzymes[40]. The plasticity of the PALPs is likely to be important for realigning the effector-secretory axis of DETC according to the mode of tissue stress.

Our results show that the adhesiveness of PALPs is triggered by TCR and mediated in part by the epithelial integrin CD103, a scenario that is consistent with a morphogenic role for CD103 in DETCs[28]. The observed *in vivo* increase of CD103 expression on *Tcrd*$^{-/-}$ DETCs is consistent with the negative control of this integrin expression by DETC TCR activation[17]. However, the kinetics of dendrite detachment that we observed in response to acute stress was fast, and the impact of CD103 deficiency upon dendrite anchoring incomplete; therefore, we propose that γδ TCR regulates cell attachment in part by modulating the clustering and/or inside-out affinity of this and, considering the recruitment of LFA-1 to PALPs, other integrins.

In summary, we have uncovered *in vivo* an immunological synapse-like activatory interaction that is uniquely sustained at steady state in normal epidermis by the monomorphic, epidermis-associated $V_{\gamma}5$ TCR. The finding of $V_{\gamma}5$-like reactivity amongst rare αβ DETCs suggests a capacity of certain αβ TCRs to mimic the specificity of epithelial γδ TCR. Based on these results, the search for the elusive epithelial TCR ligands should include physiologically expressed molecules, in addition to stress-upregulated ones. The physiological roles for γδ TCR autoreactivity are likely to be multiple, ranging from those documented here, such as the pro-active targeting of T cell surveillance at barrier-forming tight junctions, to more speculative ideas, such as homeostasis-regulating inter-cellular communication and ligand pattern-based stress detection.

## METHODS

### Mice

C57BL/6 albino mice were obtained from the National Cancer Institute (Frederick, MD), *Tcrd*$^{-/-}$, *Itgae*$^{-/-}$ mice from Jackson Labs (Bar Harbor, ME), and CD11c-YFP mice from M. Nussenzweig (The Rockefeller University, NY). IL2p8-GFP mice from M. Yui and E. Rothenberg (Caltech, CA) were crossed with C57BL/6-albino mice to produce white-coated mice and those mice were further crossed with the *Tcrd*$^{-/-}$, *Itgae*$^{-/-}$ or CD11c-YFP mice to introduce the IL2p8-GFP reporter gene onto those backgrounds. Whole ears from the DAP10$^{/}$DAP12 double knock-out mice were provided by L. Lanier (UCSF; CA). The animal care was delivered in accordance with the UT MD Anderson Institutional Animal Care and Use Committee guidelines.

### Intravital dynamics-immunosignal correlative microscopy in the skin

IL2p8-GFP, *Tcrd*$^{-/-}$/IL2p8-GFP, *Itgae*$^{-/-}$/IL2p8-GFP or CD11c-YFP/IL2p8-GFP mice were anesthetized by isoflurane inhalation. The ear pinna was immobilized on a heated stage with a dab of silicone paste, and the ventral surface was moistened with a drop of PBS and covered with a 0.17-mm glass cover slip for imaging through a piezoelectric Z-drive-mounted (Piezosystem Jena, Inc., Hopedale, MA) 20x NA 0.7 dry objective on an upright Leica SP5 RS resonant scanning confocal/multiphoton microscope (Leica Microsystems,

Inc., Bannockburn, IL). Stacks of 30-40 images, spaced 0.1-1 μm apart, were acquired every 1-3 minutes. In some experiments where the dermis was injected with fluorescent reagents and for CD11c-YFP/IL2p8-GFP mice, sequential excitation was used to prevent spectral bleed-through, which was verified using singly fluorescing specimens. Line or frame averaging and a post-acquisition kernel 3 median filter were used to reduce noise. Cell motility was recorded for 30 min to several hours. For long-term analysis, the procedure was repeated every 12 h for 28 days. Immediately after the last intravital recording, the mice were euthanized and the skin was excised, fixed, and analyzed by immunofluorescence, as described below. The same area was located in both data sets based on landmark features, and the video recordings were aligned with the immunofluorescence images using the Stackreg plugin[41] in the ImageJ software (National Institutes of Health, Bethesda, MD) and further analyzed with the Slidebook 4.2 software (3I, Denver, CO). Two-dimensional projections were generated by maximum intensity, and to visualize depth, one channel was represented as a color-coded depth projection using the Leica Application Suite Advanced Fluorescence software. Additional image and dynamics analyses were performed with Slidebook 4.2 and ImageJ as detailed in the Supplementary Methods.

## Immunofluorescence

Mouse ears were split laterally and immediately fixed for 1 h with 4% formaldehyde at room temperature. Alternatively, tissues were immersed in ice-cold 4% formaldehyde for 30 min followed by 30 min at room temperature with similar results upon TCR and phosphotyrosine morphology retention. For the DAP10/12 double knock-out mice, whole ears were immersed in 4% formaldehyde for 2 h and split 24 h later. The subcutaneous cartilage was removed and the skin was permeabilized for at least 18 h with 0.5% (w/v) saponin, 0.2% Triton-X100 in 2% fetal bovine serum (FBS), and 0.03% azide in phosphate-buffered saline (PBS). Triton-X100 was omitted for CTB and LAMP-1 staining. For NKG2D and $V_{\gamma}5$ polarization analysis, the epidermal sheets were isolated using 0.5 M $NH_4SCN$ (30 min at 37°C) and fixed with ice-cold acetone. The samples were stained with antibodies (listed in Supplementary Methods) in 2% FBS-0.5% saponin in PBS at 22-37°C for 5-18 h and, after being washed in PBS, mounted in ProlongGold (Invitrogen, Carlsbad, CA). To verify staining specificity, we used isotype-matched antibodies and, for CD3ζ, γδ TCR, $V_{\gamma}5$ TCR, and CD103, the corresponding knock-out mice. The specificity of anti-pY staining was confirmed using samples pre-treated with Antarctic phosphatase (25 units/30 μl, 4 h, 37°C; New England Biolabs, Ipswich, MA). Fluorescence microscopy was performed using the SP5 RS (resonant) confocal or SP2 SE laser-scanning confocal microscopes with 40× oil (NA 1.25), or 63× oil (NA 1.4) objectives (Leica Microsystems, Inc., Bannockburn, IL). All multichannel images were recorded using sequential excitation. The lack of spectral bleed-through was ascertained using singly fluorescing specimens, and if detected, linear un-mixing was performed.

## Flow cytometry

Mice were shaved, depilated with Nair cream (Church & Dwight Co., Inc., Princeton, NJ), and the back skin was dissected and incubated for 1.5 h at 37 °C in dispase II solution (2.5 mg/ml, STEMCELL Technologies Inc., Vancouver, BC, Canada). The epidermis was separated and further disaggregated in TrypLE Select (Invitrogen). The cell suspensions

were filtered, washed, and resuspended in PBS with 2% FBS and 0.03% azide. After blocking with the anti-FcR antibody (CD16-CD32, BD Pharmingen, San Diego, CA), the cells were stained with the appropriate antibodies and analyzed by flow cytometry using FACSCalibur (BD Biosciences, San Jose, CA). The data were analyzed with FlowJo 7.6.1 (Tree Star, Inc., Ashland, OR) or Cyflogic 1.2.1 (CyFlo Ltd, Turku, Finland).

### DETC activation *in vitro* and *in vivo*

These procedures are described in the Supplementary Methods.

### Statistical analysis

The statistical analysis and exponential decay modeling were performed with GraphPad Prism version 5.00 for Windows (GraphPad Software, San Diego, CA). The box graphs in the figures show interquartile distance with Tukey whiskers. The statistical significance of the differences between the experimental groups was determined with a non-parametric Mann-Whitney U-test (2-group comparison) or Kruskal-Wallis test followed by the Dunn's multiple comparison test (3 or more groups), unless otherwise stated. P values less than 0.05 were considered significant.

## Supplementary Material

Refer to Web version on PubMed Central for supplementary material.

## Acknowledgements

We thank W. Havran for the 7-17 cell line and advice; E. Rothenberg and M. Yui for the IL2p8-GFP mice; M. Nussenzweig for the CD11c-YFP mice; L. Lanier, J. Beilke and M. Orr for tissue samples from DAP10/DAP12 double knock-out mice; N. R.J. Gascoigne, G. Fu, D. Zhou and W. Swat for other mutant mice (data not shown); A. Fukunaga for help with tissue processing; D. Nevozhay for help with statistical analysis; and M. Kripke, S. Watowich, C. Zhu, S.Ullrich, K. Newberry, W. Pagel, and members of the Zal lab for valuable comments on the manuscript. This work was funded by grants from the National Institute of Allergy and Infection Diseases (K22-AI065688 to TZ), MD Anderson Cancer Center (3-0026138 to TZ), and the National Cancer Institute (Cancer Center Support Grant CA016672 to MD Anderson). This work was also funded in part by institutional startup funds (TZ).

## REFERENCES

1. Girardi M, et al. Regulation of cutaneous malignancy by gammadelta T cells. Science. 2001; 294:605–609. [PubMed: 11567106]
2. Jameson J, et al. A role for skin gammadelta T cells in wound repair. Science. 2002; 296:747–749. [PubMed: 11976459]
3. Chen Y, Chou K, Fuchs E, Havran WL, Boismenu R. Protection of the intestinal mucosa by intraepithelial gamma delta T cells. Proc Natl Acad Sci U S A. 2002; 99:14338–14343. [PubMed: 12376619]
4. Girardi M, Lewis JM, Filler RB, Hayday AC, Tigelaar RE. Environmentally responsive and reversible regulation of epidermal barrier function by gammadelta T cells. J Invest Dermatol. 2006; 126:808–814. [PubMed: 16439970]
5. Carding SR, Egan PJ. Gammadelta T cells: functional plasticity and heterogeneity. Nat Rev Immunol. 2002; 2:336–345. [PubMed: 12033739]
6. Xiong N, Raulet DH. Development and selection of gammadelta T cells. Immunol Rev. 2007; 215:15–31. [PubMed: 17291276]

7. Bandeira A, et al. Localization of gamma/delta T cells to the intestinal epithelium is independent of normal microbial colonization. J Exp Med. 1990; 172:239–244. [PubMed: 2141628]
8. Groh V, Steinle A, Bauer S, Spies T. Recognition of stress-induced MHC molecules by intestinal epithelial gammadelta T cells. Science. 1998; 279:1737–1740. [PubMed: 9497295]
9. Havran WL, Chien YH, Allison JP. Recognition of self antigens by skin-derived T cells with invariant gamma delta antigen receptors. Science. 1991; 252:1430–1432. [PubMed: 1828619]
10. Diefenbach A, Jamieson AM, Liu SD, Shastri N, Raulet DH. Ligands for the murine NKG2D receptor: expression by tumor cells and activation of NK cells and macrophages. Nat Immunol. 2000; 1:119–126. [PubMed: 11248803]
11. Strid J, et al. Acute upregulation of an NKG2D ligand promotes rapid reorganization of a local immune compartment with pleiotropic effects on carcinogenesis. Nat Immunol. 2008; 9:146–154. [PubMed: 18176566]
12. Hayday AC. Gammadelta T cells and the lymphoid stress-surveillance response. Immunity. 2009; 31:184–196. [PubMed: 19699170]
13. Whang MI, Guerra N, Raulet DH. Costimulation of dendritic epidermal gammadelta T cells by a new NKG2D ligand expressed specifically in the skin. J Immunol. 2009; 182:4557–4564. [PubMed: 19342629]
14. Havran WL, Allison JP. Developmentally ordered appearance of thymocytes expressing different T-cell antigen receptors. Nature. 1988; 335:443–445. [PubMed: 2458531]
15. Barbee SD, et al. Skint-1 is a highly specific, unique selecting component for epidermal T cells. Proc Natl Acad Sci U S A. 2011; 108:3330–3335. [PubMed: 21300860]
16. Boyden LM, et al. Skint1, the prototype of a newly identified immunoglobulin superfamily gene cluster, positively selects epidermal gammadelta T cells. Nat Genet. 2008; 40:656–662. [PubMed: 18408721]
17. Jameson JM, Cauvi G, Witherden DA, Havran WL. A keratinocyte-responsive gamma delta TCR is necessary for dendritic epidermal T cell activation by damaged keratinocytes and maintenance in the epidermis. J Immunol. 2004; 172:3573–3579. [PubMed: 15004158]
18. Hara H, et al. Development of dendritic epidermal T cells with a skewed diversity of gamma delta TCRs in V delta 1-deficient mice. J Immunol. 2000; 165:3695–3705. [PubMed: 11034374]
19. Mallick-Wood CA, et al. Conservation of T cell receptor conformation in epidermal gammadelta cells with disrupted primary Vgamma gene usage. Science. 1998; 279:1729–1733. [PubMed: 9497293]
20. Minagawa M, et al. Homogeneous epithelial gamma delta T cell repertoire of the skin is shaped through peripheral selection. J Dermatol Sci. 2001; 25:150–155. [PubMed: 11164711]
21. Yui MA, Sharp LL, Havran WL, Rothenberg EV. Preferential activation of an IL-2 regulatory sequence transgene in TCR gamma delta and NKT cells: subset-specific differences in IL-2 regulation. J Immunol. 172:4691–4699. [PubMed: 15067044]
22. Hogquist KA, et al. T cell receptor antagonist peptides induce positive selection. Cell. 1994; 76:17–27. [PubMed: 8287475]
23. Mombaerts P, et al. RAG-1-deficient mice have no mature B and T lymphocytes. Cell. 1992; 68:869–877. [PubMed: 1547488]
24. Chiba H, Osanai M, Murata M, Kojima T, Sawada N. Transmembrane proteins of tight junctions. Biochim Biophys Acta. 2008; 1778:588–600. [PubMed: 17916321]
25. Lanier LL. DAP10- and DAP12-associated receptors in innate immunity. Immunol Rev. 2009; 227:150–160. [PubMed: 19120482]
26. Chan AC, et al. Activation of ZAP-70 kinase activity by phosphorylation of tyrosine 493 is required for lymphocyte antigen receptor function. The EMBO journal. 1995; 14:2499–2508. [PubMed: 7781602]
27. Kersh EN, Shaw AS, Allen PM. Fidelity of T cell activation through multistep T cell receptor zeta phosphorylation. Science. 1998; 281:572–575. [PubMed: 9677202]
28. Schlickum S, et al. Integrin alpha E(CD103)beta 7 influences cellular shape and motility in a ligand-dependent fashion. Blood. 2008; 112:619–625. [PubMed: 18492951]

29. Schon MP, et al. Mucosal T lymphocyte numbers are selectively reduced in integrin alpha E (CD103)-deficient mice. J Immunol. 1999; 162:6641–6649. [PubMed: 10352281]
30. Dustin ML, Chakraborty AK, Shaw AS. Understanding the structure and function of the immunological synapse. Cold Spring Harb Perspect Biol. 2010; 2
31. Freiberg BA, et al. Staging and resetting T cell activation in SMACs. Nat Immunol. 2002; 3:911–917. [PubMed: 12244310]
32. Stinchcombe JC, Bossi G, Booth S, Griffiths GM. The immunological synapse of CTL contains a secretory domain and membrane bridges. Immunity. 2001; 15:751–761. [PubMed: 11728337]
33. Mobius W, Herzog V, Sandhoff K, Schwarzmann G. Intracellular distribution of a biotin-labeled ganglioside, GM1, by immunoelectron microscopy after endocytosis in fibroblasts. J Histochem Cytochem. 1999; 47:1005–1014. [PubMed: 10424884]
34. Parton RG. Ultrastructural localization of gangliosides; GM1 is concentrated in caveolae. J Histochem Cytochem. 1994; 42:155–166. [PubMed: 8288861]
35. Witherden DA, et al. The junctional adhesion molecule JAML is a costimulatory receptor for epithelial gammadelta T cell activation. Science. 2010; 329:1205–1210. [PubMed: 20813954]
36. Saito T, Yokosuka T, Hashimoto-Tane A. Dynamic regulation of T cell activation and co-stimulation through TCR-microclusters. FEBS Lett. 2010; 584:4865–4871. [PubMed: 21110974]
37. Campi G, Varma R, Dustin ML. Actin and agonist MHC-peptide complex-dependent T cell receptor microclusters as scaffolds for signaling. J Exp Med. 2005; 202:1031–1036. [PubMed: 16216891]
38. Komano H, et al. Homeostatic regulation of intestinal epithelia by intraepithelial gamma delta T cells. Proc Natl Acad Sci U S A. 1995; 92:6147–6151. [PubMed: 7597094]
39. Sharp LL, Jameson JM, Cauvi G, Havran WL. Dendritic epidermal T cells regulate skin homeostasis through local production of insulin-like growth factor 1. Nat Immunol. 2005; 6:73–79. [PubMed: 15592472]
40. Mohamadzadeh M, et al. Functional roles for granzymes in murine epidermal gamma(delta) T-cell-mediated killing of tumor targets. J Invest Dermatol. 1996; 107:738–742. [PubMed: 8875959]
41. Thévenaz P, Ruttimann UE, Unser M. A Pyramid Approach to Subpixel Registration Based on Intensity. IEEE Transactions on Image Processing. 1998; 7:27–41. [PubMed: 18267377]
42. Kubo A, Nagao K, Yokouchi M, Sasaki H, Amagai M. External antigen uptake by Langerhans cells with reorganization of epidermal tight junction barriers. J Exp Med. 2009; 206:2937–2946. [PubMed: 19995951]
43. Leupin O, Zaru R, Laroche T, Muller S, Valitutti S. Exclusion of CD45 from the T-cell receptor signaling area in antigen-stimulated T lymphocytes. Curr Biol. 2000; 10:277–280. [PubMed: 10712909]
44. Kuziel WA, et al. Regulation of T-cell receptor gamma-chain RNA expression in murine Thy-1+ dendritic epidermal cells. Nature. 1987; 328:263–266. [PubMed: 2885757]
45. Baxter CS, Andringa A, Chalfin K, Miller ML. Effect of tumor-promoting agents on density and morphometric parameters of mouse epidermal Langerhans and Thy-1+ cells. Carcinogenesis. 1991; 12:1017–1021. [PubMed: 1675159]

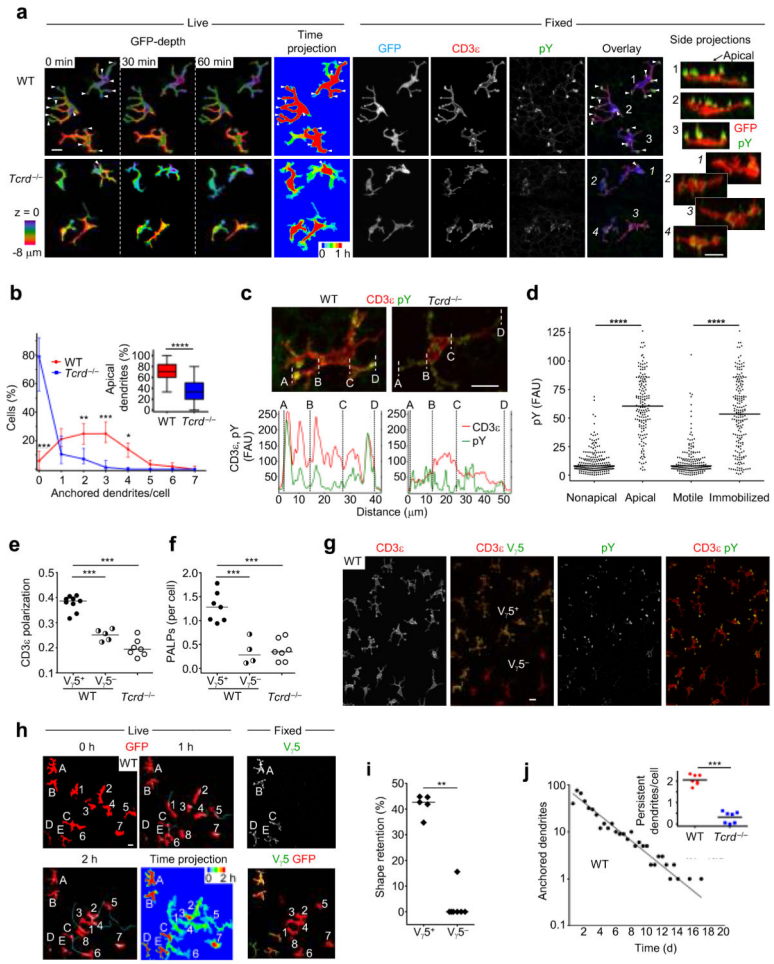


**Figure 1. DETCs are anchored in apical epidermis at steady-state through phosphotyrosine-rich aggregates located on projections in a manner dependent on $V_\gamma5$ TCR**

(**a**) Intravital dynamics-immunofluorescence correlative confocal microscopy showing the correlation of DETC dendrite immobilization *in vivo* (left panels, 'Live') with TCR/CD3ε and pY content (right panels, 'Fixed') in the same DETCs in healthy ear skin in wild-type (WT) or *Tcrd*$^{-/-}$ IL2p8-GFP reporter mice (Supplementary Video 3). Time projection represents in red the cell areas that were immobilized for 60 min. The arrowheads indicate the stationary dendrites. Overlay: CD3ε (red), pY (green) and GFP (blue). Far right: Side projections of the indicated DETCs, showing pY (green) and GFP (red). (**b**) Enumeration of DETCs according to the number of anchored and apically oriented dendrites in wild-type and *Tcrd*$^{-/-}$ IL2p8-GFP mice during at least 1 h of intravital visualization. n=498 (wild-type) and 524 (*Tcrd*$^{-/-}$) DETCs in 6-7 mice per strain. Inset: Fraction of dendrites extending above the cell's mid-body in wild-type or *Tcrd*$^{-/-}$ mice. n=77 (wild-type) and n=80 (*Tcrd*$^{-/-}$) cells in three mice per strain. (**c**) Top: Confocal microscopy of non-treated skin biopsies from wild-type and *Tcrd*$^{-/-}$ mice stained for CD3ε chains (red) and pY (green). Below: Profiles of CD3ε and pY fluorescence intensity along the cell membrane between the dashed lines. FAU, fluorescence arbitrary units. (**d**) pY content at dendrite endings in apical versus non-apical and mobile versus immobilized dendrites in wild-type skin

quantified in n=371 dendrite ends in 71 cells. (**e**) Polarization of TCR/CD3ε into ends of dendrites expressed as index (calculation method described in Supplementary Information) in $V_\gamma5^+$ and $V_\gamma5^-$ wild-type and *Tcrd*$^{-/-}$ DETCs. Each symbol represents one mouse. Cumulative n=5375 ($V_\gamma5^+$ WT), 262 ($V_\gamma5^-$ WT), and 3528(*Tcrd*$^{-/-}$) cells. (**f**) Frequency of PALPs in $V_\gamma5^+$ and $V_\gamma5^-$ wild-type and *Tcrd*$^{-/-}$ DETCs at steady-state. Cell numbers as in **e**, except for $V_\gamma5^-$ WT, where 245 cells were analyzed. (**g**) Confocal maximum intensity projection microscopy of wild-type skin stained for CD3ε (red) and $V_\gamma5$ or pY (green in overlaid images) showing an area of skin containing both $V_\gamma5^-$ DETCs (αβ or γδ TCRs) and $V_\gamma5^+$ DETCs. (**h**) Frames from a 2 h intravital video (Supplementary Video 5) recorded in a wild-type IL2p8-GFP mouse followed by $V_\gamma5$ TCR staining. Letters: individual $V_\gamma5^-$ DETCs. Numbers: $V_\gamma5^+$ DETCs. Blue lines: cell tracks. (**i**) Cell shape retention in $V_\gamma5^+$ and $V_\gamma5^-$ wild-type DETCs assessed in wild-type skin (calculation method described in Supplementary Information). n=5 ($V_\gamma5^+$) and n=7 ($V_\gamma5^-$), based on **h** (**j**) Number of anchoring points persisting in the same location for the indicated number of days as assessed by live imaging (Supplementary Video 6) in a wild-type mouse (n=47). Inset: average number of dendrites anchored for 24 h in wild-type and *Tcrd*$^{-/-}$ mice. Each dot is the average from one field of view; the lines are the overall means. n=189 (wild-type) and 195 (*Tcrd*$^{-/-}$) in at least three mice per strain. Scale bars, 10 μm. Data show one representative of at least two independent experiments. In **b**, **d**, **e**, **f**, **j**/inset data was pooled. Horizontal graph bars = medians; *P < 0.05, **P < 0.01, ***P < 0.001, ****P < 0.0001 (in all figures); two-way ANOVA test in **b**.

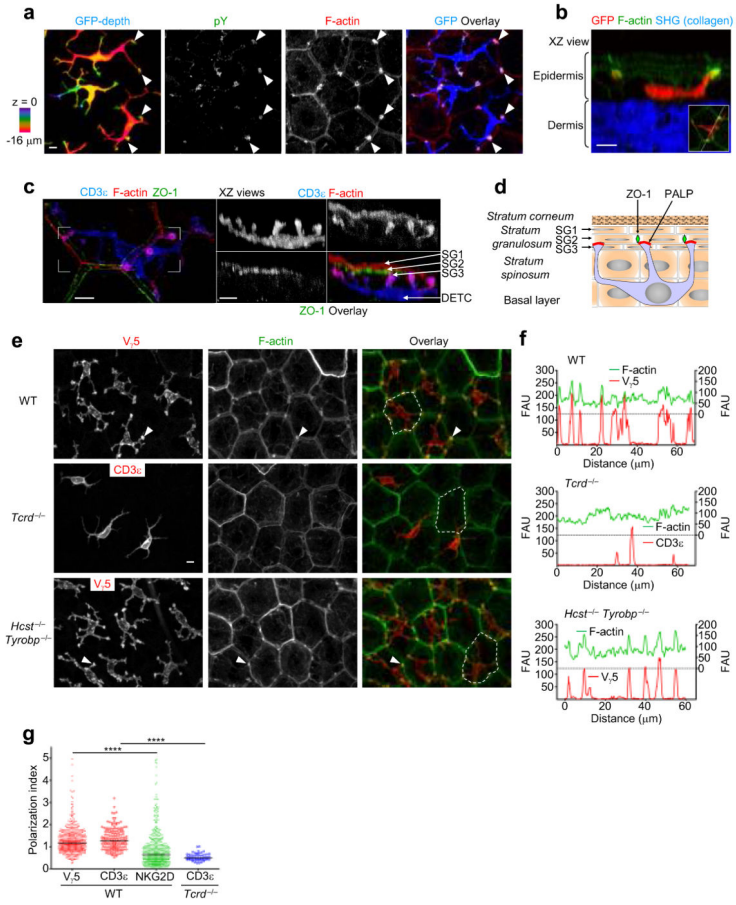


**Figure 2. DETCs in wild-type mice are targeted through the PALPs at the squamous keratinocyte junctions dependent on γδ TCR and independent of NKG2D**

(**a**) Confocal microscopy of a non-treated skin biopsy from a wild-type IL2p8-GFP mouse stained for pY (green) and F-actin (red); GFP-blue. Arrowheads: Apical dendrites with pY and F-actin aggregates. (**b**) Side view showing F-actin cluster localization (green) on apical dendrites (GFP, red) in the IL2p8-GFP skin along the line in the lateral view inset. Dermal collagen (blue) was revealed by multiphoton second harmonic generation (SHG). (**c**) 3D confocal microscopy of TCR/CD3ζ (blue) and F-actin cluster positioning with respect to ZO-1 (green) in wild-type epidermis. XZ views are side projections from a confocal stack volume delineated in the XY view (**d**) A model of DETC interaction with the apical epidermis through the PALPs (layers named according to a prior report[42]). (**e**) Confocal microscopy of non-treated skin biopsies from wild-type, *Tcrd*$^{-/-}$ and DAP10/12 double knock-out (*Hcst*$^{-/-}$, *Tyrobp*$^{-/-}$) mice stained for $V_\gamma5$/CD3ε (green) and F-actin (green). The arrowheads indicate examples of $V_\gamma5$/CD3ε and inter-keratinocyte junction colocalization. (**f**) Fluorescence image densitometry of $V_\gamma5$/CD3ε and F-actin (left and right axis, respectively) along the dashed lines in **e**. (**g**) *In situ* NKG2D and $V_\gamma5$/CD3ε polarization in wild-type and *Tcrd*$^{-/-}$ DETCs (calculation method described in Supplementary Information). Each dot represents a single dendrite. n=476 dendrites in three wild-type mice ($V_\gamma5$ vs. NKG2D), and 155 (wild-type) and 60 (*Tcrd*$^{-/-}$) dendrites (CD3ε). Scale bars, 5 µm.

Data show one representative of at least two independent experiments. Confocal images are maximum intensity projections.

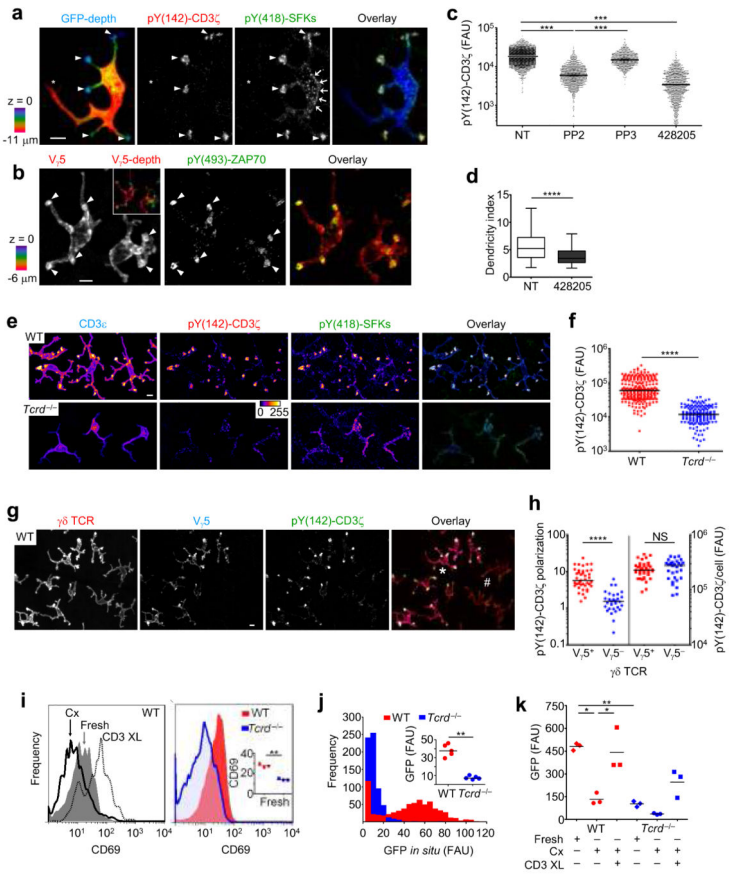


**Figure 3. $V_\gamma5$ TCR is activated in PALPs and maintains DETCs in an activated state *in vivo***

(**a**, **b**) 3D confocal microscopy of DETCs in non-treated skin biopsies from wild-type IL2p8-GFP (**a**) and C57BL/6 (**b**) mice stained for the indicated pY signaling intermediates. DETCs were visualized by GFP signal (blue in **a**) or anti-$V_\gamma5$ staining (red in **b**). The arrowheads indicate the apical dendrites, the asterisk marks a horizontal dendrite, and the arrows show microclusters of $pY^{418}$-SFKs in the mid-body. (**c**, **d**) Image cytometry of $pY^{142}$-CD3ζ and cell morphometry of DETCs in wild-type ear skin biopsies treated with kinase inhibitors (calculation method described in Supplementary Information). NT, not treated. N=3148 (NT), 1220 (PP2), 873 (PP3), and 1307 (Lck inhibitor 428205). (**e**) Confocal microscopy of non-treated wild-type and *Tcrd*$^{-/-}$ skin biopsies stained for CD3ε (blue), $pY^{142}$-CD3ζ (red) and $pY^{418}$-SFKs (green). Individual fluorescence channels are rendered in a fire color scale. (**f**) Image cytometry of $pY^{142}$-CD3ζ content in n=228 (wild-type) and 147 (*Tcrd*$^{-/-}$) DETCs *in situ* pooled in three mice per strain. (**g**) Confocal microscopy of a non-treated wild-type skin stained for γδ TCR (red), $V_\gamma5$ (blue) and $pY^{142}$-CD3ζ(green) selected to contain $V_\gamma5^+$ (asterisk) and $V_\gamma5^-$ γδ $TCR^+$ (#) DETCs. (**h**) Image cytometry of $pY^{142}$-CD3ζ polarization (left) and whole-cell content (right) in $V_\gamma5^+$ and $V_\gamma5^-$ DETCs in wild-type skin, n=41 ($V_\gamma5^+$) and 30 ($V_\gamma5^-$ γδ $TCR^+$) cells. NS, not significant. (**i**) Flow cytometry of CD69 levels. Left: in wild-type DETCs after *in vitro* culture only (Cx), with CD3ε cross-linking (CD3 XL), or freshly isolated. Right: Freshly isolated DETCs from wild-type or *Tcrd*$^{-/-}$ epidermis gated on Thy1.2$^+$. Inset: mean CD69 fluorescence intensity

in three mice per strain; bars=overall means; (**j**) Confocal image cytometry of *in situ* GFP intensity in DETCs in non-treated wild-type and *Tcrd*$^{-/-}$ skin biopsies from IL2p8-GFP mice. Cell bodies were revealed by anti-CD3ε counterstaining. Inset: median GFP levels per DETC. n=3048 (wild-type) and 1834 (*Tcrd*$^{-/-}$) cells in five mice per strain. (**k**) Flow cytometry of GFP levels in wild-type and *Tcrd*$^{-/-}$ IL2p8-GFP DETCs, fresh or after *in vitro* culture with (CD3 XL), or without (Cx) CD3ε cross-linking. Each dot represents the mean signal from one mouse; bars=overall means. Scale bars, 5 μm. Data show one representative of at least two independent experiments. Data in panels **i** and **k** were analyzed with Student's t-test. Images are 3D maximum intensity projections.

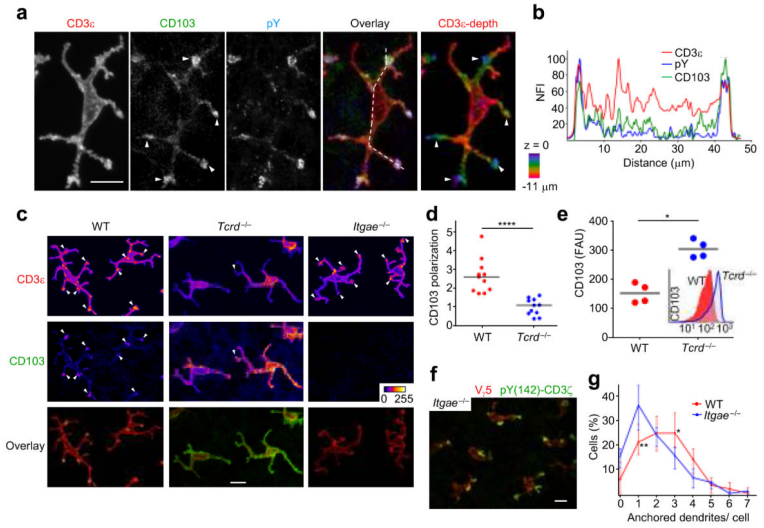


**Figure 4. γδ TCR mediates dendrite attachment through CD103**

(**a**) 3D confocal microscopy of a DETC in a non-treated skin biopsy from a wild-type mouse stained for CD3ε (red), pY (blue) and CD103 (green). The arrowheads indicate CD3ε and CD103 clusters in apical dendrites. Depth is represented in a color scale. (**b**) Image densitometry along the dashed line in **a**. NFI, normalized fluorescence intensity. (**c**) Confocal microscopy of CD103 (green) in non-treated skin biopsies from wild-type, CD103-deficient (*Itgae*$^{-/-}$), and *Tcrd*$^{-/-}$ mice counter-stained for CD3ε (red) (single channels rendered in a fire color scale). (**d**) Image morphometry of CD103 polarization index within dendrites in skin-resident wild-type and *Tcrd*$^{-/-}$ DETCs; n=11 apical dendrites in each strain in 5-8 cells. (**e**) Flow cytometry of CD103 levels in DETCs freshly isolated from wild-type and *Tcrd*$^{-/-}$ mice. Dots: means from individual mice, bars=overall means. The inset shows representative histograms. (**f**) Confocal microscopy of a non-treated skin biopsy from a CD103-deficient mouse stained for $V_\gamma5$ (red) and pY$^{142}$-CD3ζ (green). (**g**) Intravital time-lapse microscopy of dendrite dynamics in wild-type and CD103-deficient IL2p8-GFP $V_\gamma5^+$ DETCs in non-treated mice during at least 1 h; n=498 (wild-type) and 442 (*Itgae*$^{-/-}$) DETCs in 6 mice per strain and analyzed with two-way ANOVA test. Scale bars, 10 μm. Data show one representative of at least two independent experiments. Images are maximum intensity projections of 3D image stacks.

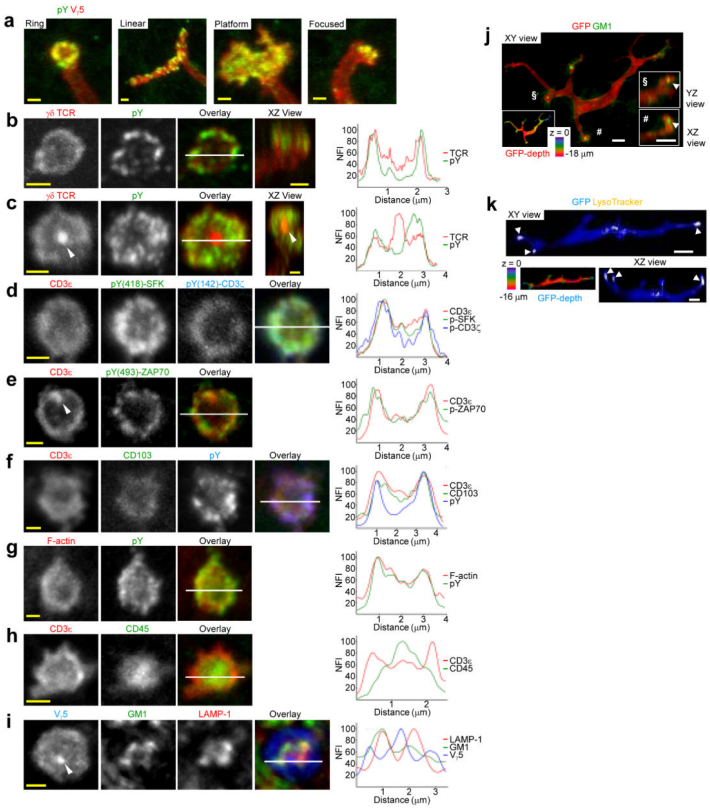


**Figure 5. PALPs display multiple hallmarks of immunological synapses**

(**a**) High-magnification confocal microscopy of PALPs in non-treated wild-type C57BL/6 skin biopsies stained for $V_{\gamma}5$ (red) and pY (green) showing the representative patterns of PALPs (frequency ± SEM): ring (40% ± 4%), linear (23% ± 4%), platform (21% ± 3%) and focused (15% ± 2%). n= 640 PALPs in five mice. (**b-i**) High-magnification confocal microscopy of ring PALPs stained for the indicated markers. Z-step = 0.2 μm. The profiles represent normalized fluorescence intensities (NFI) along the indicated lines. The arrowheads indicate a central, pY-free TCR cluster. (**j**) 3D confocal microscopy of a representative DETC in non-treated wild-type IL2p8-GFP skin stained for GM1 ganglioside (green). GFP is shown in red. Insets: magnified and side-projected dendrite endings; the arrowheads indicate $GM1^{+}$ vesicles. (**k**) Intravital visualization of lysosomes in an IL2p8-GFP DETC stained with intradermaly-injected Lysotracker dye (yellow). GFP signal is shown in blue. Yellow scale bars, 1 μm; white scale bars, 5 μm. Images show maximum intensity projections and are representative of at least two independent experiments.

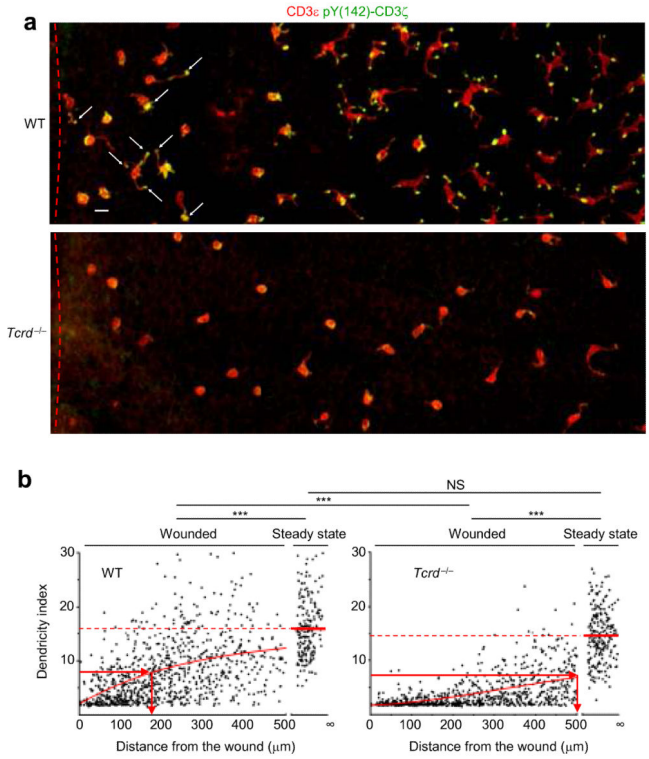


**Figure 6. γδ TCR sustains dendrite outreach upon trauma**

(**a**) Confocal microscopy of sterile punch-proximal areas (within a 500 μm zone) in the skin of wild-type and *Tcrd*$^{-/-}$ mice stained for CD3ε (red) and pY$^{142}$-CD3ζ (green) 24 h after the wounding. The dashed lines indicate wound borders and the arrows show PALP-containing dendrites on wound-margin DETCs. (**b**) Image morphometry of wild-type and *Tcrd*$^{-/-}$ DETCs 24 h after sterile wounding showing the dendricity index as a function of the distance from wound borders. Dots: individual cells. Red curves: nonlinear third-order fits; Dashed lines: medians at a steady-state. Red arrow: the distance at the half-maximum dendricity index. n=1239 (wild-type) and 1138 (*Tcrd*$^{-/-}$) cells from three mice per group. Scale bars, 10 μm. Data show one representative of at least two independent experiments.

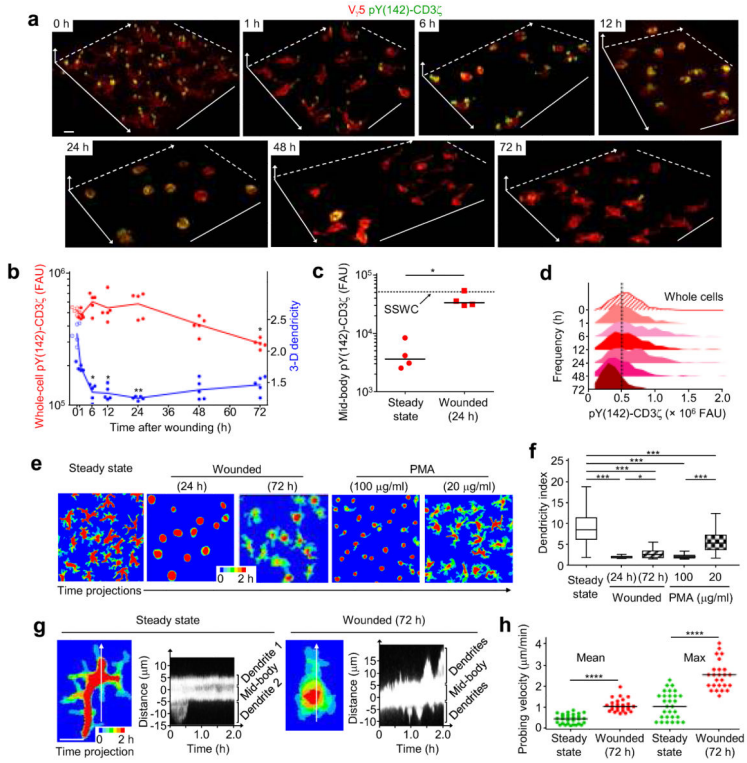


**Figure 7. Tissue stress induces TCR signal re-localization**

(**a**) Confocal microscopy of sterile punch-proximal areas (within a 300-μm zone) in the skin of wild-type mice stained for $V_\gamma5$ (red) and $pY^{142}$-CD3ζ (green) at the indicated time points after the wounding (rendered in a 3D perspective). The 0 h time point shows untreated skin. (**b**) Image cytometry of 3D data as in **a** showing quantification of $pY^{142}$-CD3ζ content (red dots, left axis) in DETCs and DETC morphology (blue dots, right axis) after wounding over time. Each dot represents the median whole-cell value from one mouse (on average 80 cells/mouse). The line connects the group's means; the statistical comparisons with the "0 h". (**c**) Quantification of $pY^{142}$-CD3ζ levels in DETC mid-bodies at steady state or 24 h after wounding (based on 2D maximum intensity projection image cytometry). n=301 (steady state) and 420 (wounded) cells; each dot represents the median value from one mouse. SSWC, steady state whole cell level. (**d**) Distribution of whole-cell $pY^{142}$-CD3ζ levels in wound-margin DETCs over time analyzed by image cytometry of data as in **b** showing pooled cells from five mice per time point. The dashed line indicates the median $pY^{142}$-CD3ζ level in non-wounded skin. (**e**) Time projections of 2-h intravital DETC dynamics recorded at steady state, after punch biopsy (24 and 72 h later), or 24 h after topical application of PMA (100 and 20 μg/ml) (Supplementary Video 7). (**f**) Image cytometry showing quantification of DETC morphology after different modes of tissue stress. The dendricity indices from at least 83 cells from two to three mice per group. (**g**, **h**) Quantification of dendrite probing activity at steady state or 72 h after punch biopsy (calculation method described in Supplementary Information). Kymographs are based on 2-h intravital videos of DETC motility along the lines indicated in the time projections. The probing velocities in **h** were calculated from kymographs of 25-29 dendrites in five cells per

condition. Each dot is the mean (left) or maximum (right) velocity for one dendrite. Scale bars, 10 μm. Data show one representative of at least two independent experiments.

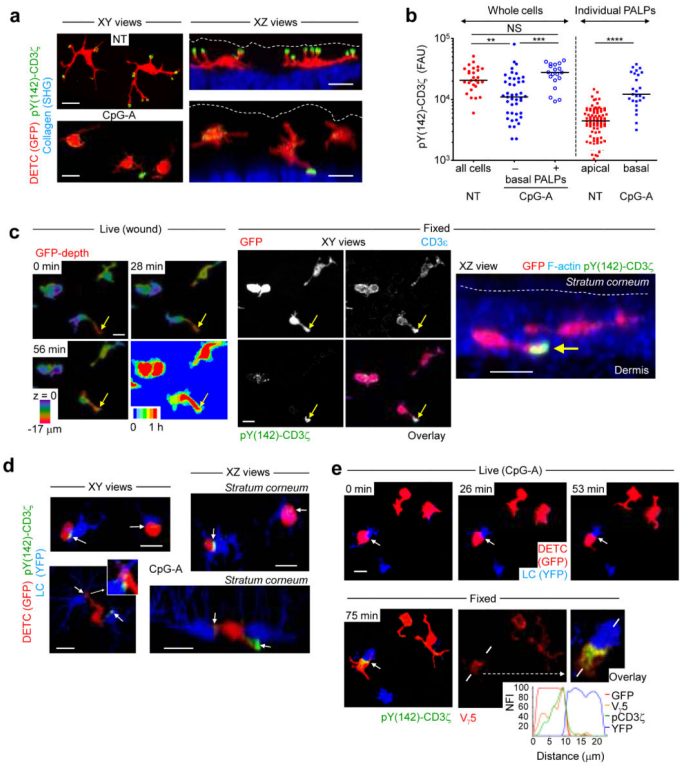


**Figure 8. Redistribution of TCR signals towards the dermis and Langerhans cells in response to inflammatory stress**

(**a**) Confocal microscopy of the wild-type skin stained for pY$^{142}$-CD3ζ (green) 9 days after intradermal injection of CpG-A in an IL2p8-GFP mouse. GFP is in red. The dermal collagen was visualized by multiphoton SHG (blue). The dashed lines indicate stratum corneum (Supplementary Video 8). The XZ views are reconstructed from stacks of confocal images. (**b**) Image cytometry of *in situ* pY$^{142}$-CD3ζ levels in DETCs performed in whole cells and in individual PALPs (apical vs. basal) in not treated (NT) or CpG-A-treated skin after 9 days. (**c**) Left: Frames of intravital visualization of wound-proximal DETCs in the wild-type IL2p8-GFP mouse skin 72 h after punch wounding (wound border not shown). The arrow indicates a downward immobilized dendrite based on depth and time projections. Right: Confocal microscopy of the same skin area recorded at left, fixed and stained for CD3ε (blue) and pY$^{142}$-CD3ζ (green) (GFP in red). The arrow points to the same downward dendrite containing a basal PALP based on the presence of CD3ε and pY$^{142}$-CD3ζ aggregates. Far right: Side projection of the DETC with the basal PALP at the epidermal-dermal junction. Epidermis is visualized by F-actin counterstaining (blue). (**d**) Confocal microscopy of the wild-type skin stained for pY$^{142}$-CD3ζ (green) 9 days after intradermal injection of CpG-A in an IL2p8-GFP/CD11c-YFP reporter mouse. GFP is in red, YFP is in blue. The arrows indicate interactions of DETCs with Langerhans cells (LC). (**e**) Top: Frames of intravital visualization of DETC-LC interaction after CpG-A treatment. The arrow shows a stable DETC-LC conjugate. Bottom: Confocal microscopy of the same skin area shown above, fixed and stained for pY$^{142}$-CD3ζ (green) and V$_\gamma$5 (red). The DETC-LC conjugate is magnified in the inset. The graph shows normalized fluorescence intensity

profiles perpendicular to the contact site. Scale bars, 10 μm. Data show one representative of at least two independent experiments.